

Tetragonal magnetic phase in $\text{Ba}_{1-x}\text{K}_x\text{Fe}_2\text{As}_2$ from x-ray and neutron diffraction

J. M. Allred,^{1,*} S. Avci,^{1,2} D. Y. Chung,¹ H. Claus,¹ D. D. Khalyavin,³ P. Manuel,³ K. M. Taddei,^{1,4} M. G. Kanatzidis,^{1,5} S. Rosenkranz,¹ R. Osborn,¹ and O. Chmaissem^{1,4}

¹*Materials Science Division, Argonne National Laboratory, Argonne, IL 60439-4845, USA*

²*Department of Materials Science and Engineering,*

Afyon Kocatepe University, 03200 Afyon, Turkey

³*ISIS Pulsed Neutron and Muon Source, Rutherford Appleton Laboratory, Chilton, Didcot OX11 0QX, United Kingdom*

⁴*Physics Department, Northern Illinois University, DeKalb, IL 60115, USA*

⁵*Department of Chemistry, Northwestern University, Evanston, IL 60208-3113, USA*

(Dated: November 12, 2018)

Combined neutron and x-ray diffraction experiments demonstrate the formation of a low-temperature minority tetragonal phase in $\text{Ba}_{0.76}\text{K}_{0.24}\text{Fe}_2\text{As}_2$ in addition to the majority magnetic, orthorhombic phase. A coincident enhancement in the magnetic $(\frac{1}{2} \frac{1}{2} 1)$ peaks shows that this minority phase is of the same type that was observed in $\text{Ba}_{1-x}\text{Na}_x\text{Fe}_2\text{As}_2$ ($0.24 \leq x \leq 0.28$), in which the magnetic moments reorient along the c -axis. This is evidence that the tetragonal magnetic phase is a universal feature of the hole-doped iron-based superconductors.

PACS numbers: 74.70.Xa, 74.25.Ha

I. INTRODUCTION

A key to understanding the pairing mechanism in the superconducting state of the iron pnictide and chalcogenide superconductors is characterizing the nature of the electronic interactions that are responsible for the competing spin-density-wave (SDW) state. The origin of the magnetic order, which is coupled to an orthorhombic distortion of the high-temperature tetragonal lattice that is often labelled ‘nematic’ order, is still debated, with a range of theoretical treatments that range from localized orbital models to weak-coupling itinerant models based on Fermi surface nesting.^{1–3}

Since it seems that, until now, each class of models could be modified to comport with the measured properties, solely studying the principal SDW state is apparently not enough to settle the dispute. Recently we have shown that a second tetragonal magnetic phase appears near the end of the SDW dome in hole-doped $\text{Ba}_{1-x}\text{Na}_x\text{Fe}_2\text{As}_2$. This was called the “ C_4 ” phase to distinguish it from the more usual stripe SDW phase, which has “ C_2 ” symmetry.^{4–6} The magnetic structure of the C_4 phase was later shown to involve a reorientation of the spins from in-plane to out-of-plane.^{7,8} The reorientation temperature, T_r , occurs well above T_c , indicating that it does not arise from a coupling of the superconducting order parameter with the other order parameters as was observed in $\text{Ba}(\text{Fe}_{1-x}\text{Co}_x)_2\text{As}_2$,⁹ but instead must be a manifestation of changes in the coupling between iron atoms. The fact that the system returns to the tetragonal symmetry of the paramagnetic phase, while remaining magnetic, puts new constraints on the set of plausible electronic ordering mechanisms. In particular, a group theory analysis shows that it may be possible to distinguish between itinerant and quasi-local orbital models through the observation of orbital order in the C_4 phase.⁸

Characterizing the C_4 SDW phase is therefore a pri-

mary concern in settling the debate on the origin of the parent C_2 SDW phase. It is important to establish whether this phase is unique to the $\text{Ba}_{1-x}\text{Na}_x\text{Fe}_2\text{As}_2$ system, or whether it is observed in other related systems, in order to decide if the inferred physics of these specific compounds are atypical or more general. Related families such as the hole-doped $\text{Ba}_{1-x}\text{K}_x\text{Fe}_2\text{As}_2$ have been extensively studied in earlier publications.^{10,11} Here we return our attention to the region near the edge of the dome of $\text{Ba}_{1-x}\text{K}_x\text{Fe}_2\text{As}_2$ using fine temperature control with both high-resolution x-rays and high-intensity neutrons. The combined analysis shows that the reentrant C_4 tetragonal phase is indeed present in the $\text{Ba}_{1-x}\text{K}_x\text{Fe}_2\text{As}_2$ phase diagram at $x = 0.24$, but not below $x = 0.22$, indicating that it is a common feature of the hole-doped ‘122’ iron compounds. It is only present as a minority phase below a first-order transition, consistent with the delicate energy balance between the C_2 and C_4 phases predicted by itinerant spin-nematic theory,² and is rapidly suppressed below the superconducting transition. We had earlier reported that the C_4 phase in $\text{Ba}_{1-x}\text{Na}_x\text{Fe}_2\text{As}_2$ exhibited a stronger competition with superconductivity than the C_2 phase,⁴ but this is the first time we have observed the complete suppression of the C_4 phase below T_c .

II. TECHNIQUES

The polycrystalline samples reported in Ref 11 were used in the new measurements. Powders were prepared by combining stoichiometric amounts of BaAs, KAs, and Fe_2As in sealed Nb tubes, which were in turn sealed in quartz tubes and fired at 1050 °C. More details can be found in the original publication.¹¹ Powder x-ray diffraction experiments (PXRD) were measured at the Advanced Photon Source, Argonne National Laboratory, on beamline 11-BM-B using the liquid helium

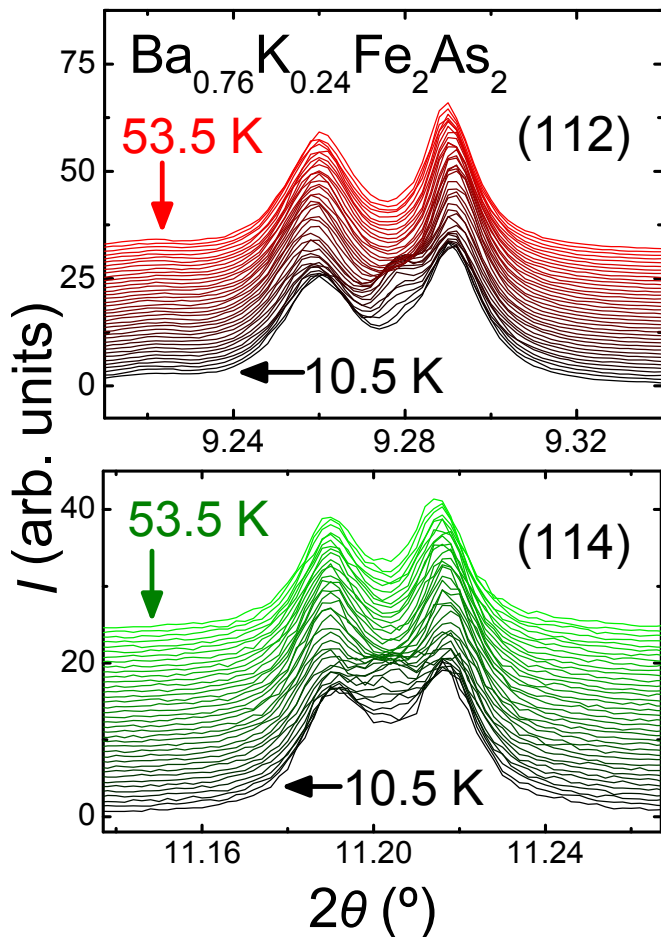


FIG. 1. Overlaid x-ray diffraction scans of $\text{Ba}_{0.76}\text{K}_{0.24}\text{Fe}_2\text{As}_2$ at approximately uniform increments from 10.5 to 53.5 K. The top panel shows the (112) reflection and the bottom shows the (114) reflection. The split peak in the orthorhombic phase corresponds to the $(11l)$ and $(\bar{1}1l)$ components (I -cell), which are the $(20l)$ and $(02l)$ peaks in the conventional F-centered cell.

cryostat ($\lambda = 0.413429 \text{ \AA}$). The sample was prepared for measurement by dusting the outside of a greased kapton capillary with sample powder. Rietveld refinements were performed using General Structure Analysis System (GSAS)¹² and the graphical user interface, EXPGUI.¹³ Powder neutron diffraction (PND) experiments were performed at ISIS, Rutherford Appleton Laboratory, on the Wish beamline.

III. RESULTS AND DISCUSSION

The diffraction data are summarized in Figures 1, 2 and 3. The peak indices are given for the body-centered tetragonal cell in all cases. The cascaded diffractograms of the x-ray diffraction data (Figure 1) shows the splitting of the (112) and (114) reflections, with clear evidence of a minority phase growing in and disappearing again

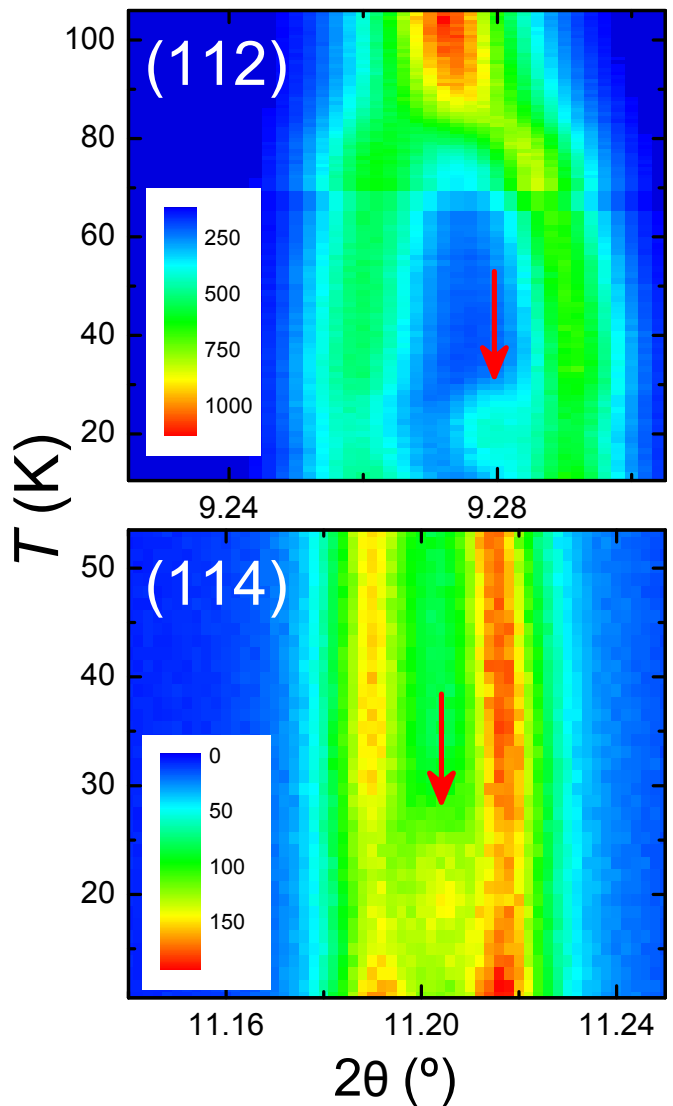


FIG. 2. False color map drawn using the x-ray diffraction data on $\text{Ba}_{0.76}\text{K}_{0.24}\text{Fe}_2\text{As}_2$. The top panel shows the temperature range from 10 to 120 K of the (112) reflection, which splits into the (202) and (022) orthorhombic peaks. The bottom panel shows the (114) (corresponding to the (204) and (024) components of the orthorhombic cell) from 10 to 53 K. The arrows point to the peak corresponding to the minority tetragonal phase.

on warming from 10 ($T_{r,1}$ to 30 K ($T_{r,2}$) between these two reflections. The same data can also be visualized using a false color map, as depicted in Figure 2. The neutron diffraction data (Figure 3) shows an evolution in the magnetic intensity within the same region for the $(\frac{1}{2}\frac{1}{2}1)$ reflection. Little change is observed in the $(\frac{1}{2}\frac{1}{2}3)$ peak. Our previous study on $\text{Ba}_{1-x}\text{Na}_x\text{Fe}_2\text{As}_2$ showed that the C_4 phase exhibits a 10-fold increase in intensity of the $(\frac{1}{2}\frac{1}{2}1)$ magnetic peak, and a slight reduction in the $(\frac{1}{2}\frac{1}{2}3)$ magnetic peak, resulting from the spin re-orientation. Here the magnitude change in the $(\frac{1}{2}\frac{1}{2}1)$ is consistent with an approximately 10% C_4 phase fraction.

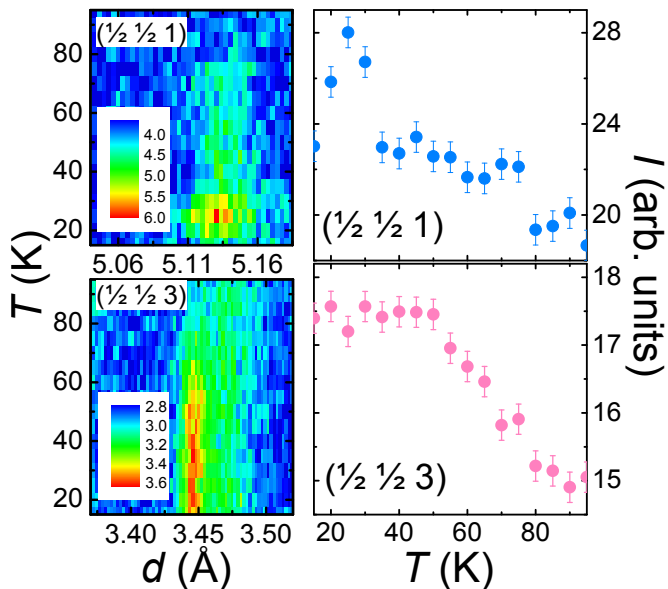


FIG. 3. Left panels: Temperature-dependent color maps depicting the magnetic peak intensity of the $(\frac{1}{2} \frac{1}{2} 1)$ (top) and $(\frac{1}{2} \frac{1}{2} 3)$ (bottom) reflections. The right panels are peak intensities integrated from a 5-point-wide cut through the peak of interest.

A two-phase Rietveld refinement was used to model the minority phase in the 11BM data. For two-overlapping phases of such similar structure, it is difficult to refine the lattice parameters for the minority phase reliably, and similar R values are obtained regardless of whether certain parameters of the tetragonal phase are constrained or allowed to refine freely. For example, freely refining the lattice parameters of the minority phase gives obviously incorrect peak positions, due to convolution with small features in the majority phase peak's shoulders that are not perfectly modeled. These values also covary with the relative phase fraction, making a unique solution unattainable. As detailed below, several assumptions and approximations must be made in order to minimize systematic errors and to produce a model that is physically meaningful.

To start, the c -axes of both phases (c_1 and c_2 , for the majority orthorhombic and minority tetragonal phases, respectively) were constrained to be equivalent, since no extra broadening of the $(00l)$ reflections was observed when comparing the two-phase and one-phase temperature regions. The shoulders in the peaks split by the orthorhombic distortion (such as what is shown in Figure 1) can then be used to define the other cell axis of the minority phase, a_2 , which allows the free refinements of a_1 and b_1 , giving good agreement with the data. Thermal and peak profile parameters of both phases are constrained to be nearly equivalent, which allowed the weight fractions to be refined self-consistently. Using this method, the final two-phase refinement models have all of the crystallographic parameters of the orthorhombic phase freely refined, while, for the tetragonal phase, only the scale

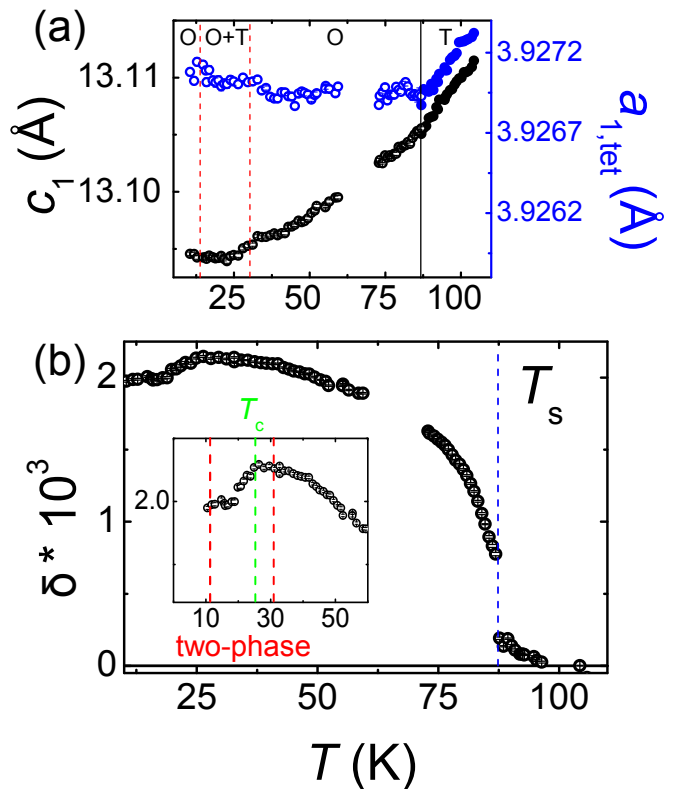


FIG. 4. (a) Refined lattice parameters for the majority phase in $\text{Ba}_{0.76}\text{K}_{0.24}\text{Fe}_2\text{As}_2$ determined from x-ray powder diffraction. Black circles represent c_1 , and blue circles represent $a_{1,\text{tet}}$ (see text). Orthorhombic and tetragonal fits were used below and above 87 K, respectively. (b) The orthorhombic order parameter ($\delta_1 = \frac{a_1 - b_1}{a_1 + b_1}$) is plotted from refinements where the majority phase is refined as orthorhombic at all temperatures for comparison. Inset is a detailed view around T_c and T_t .

factor is refined by GSAS.

The temperature dependence of the majority phase is summarized in Figures 4 and 5. The refined lattice parameters of the majority (orthorhombic) phase do not appear to be affected by the presence of the minority (tetragonal) phase. For example, the orthorhombic order parameter shows the usual discontinuity at T_c (26 K), but there is no evidence of a change in slope corresponding to the (dis)appearance of the tetragonal phase. This is further evidence that the transition from orthorhombic C_2 phase to the magnetic C_4 phase is of first order and that the two phases are microscopically decoupled. The structural transition at T_s is also clearly in the primitive basal plane lattice parameter (here, called a_{tet}) and orthorhombic order parameter, $\delta = \frac{a_1 - b_1}{a_1 + b_1}$ (Figure 4a and b, respectively). The in-plane lattice parameter, a_{tet} , is calculated from the orthorhombic phase by transforming the conventional F -centered cell back to the I -centered one, via $a_{1,\text{tet}} = \sqrt{(a_1^2 + b_1^2)}/2$. Below T_N , this value is clearly enhanced, as is typical of hole-doped 122 ironpnictides,¹⁴ while the c -axis shows little change. The vol-

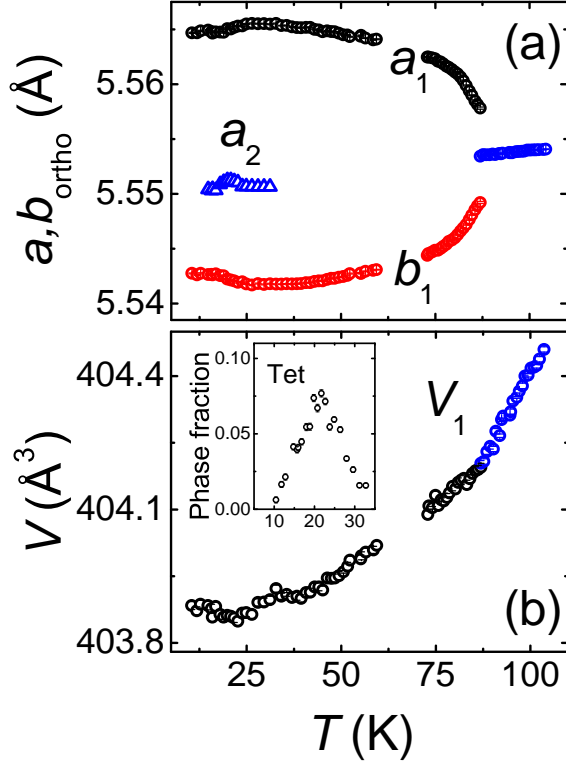


FIG. 5. (a) The splitting of the a (black circles) and b (red circles) lattice parameters in the orthorhombic phase, along with the minority phase tetragonal a_2 (blue triangles) lattice parameter. Tetragonal lattice parameters are scaled by $\sqrt{2}$. (b) The volume of the majority phase (V_1), with blue and black circles being used to demarcate the transition from tetragonal to orthorhombic models, respectively. The inset is the refined phase fraction of the minority phase, when present.

ume anomaly at T_N is primarily seen as a subtle change in slope.

The properties of the minority phase are also plotted in Figure 5. What is observed is a small tetragonal phase fraction that reaches a maximum ($\sim 8\%$) between 20.8 and 22.7 K, and becomes indistinguishable from background below 12 K and above 30 K. The in-plane lattice parameter appears to be rather smaller than the primary phase (Figure 5). The phase fraction derived from the x-ray data peaks at the same temperature as the enhancement in the magnetic peak intensity of the $(\frac{1}{2} \frac{1}{2} 1)$ reflection in neutron data. This agrees well with the interpretation that this minority phase is the same tetragonal magnetic phase that was observed in $\text{Ba}_{1-x}\text{Na}_x\text{Fe}_2\text{As}_2$.⁴

In order to draw a modified phase diagram for the $\text{Ba}_{1-x}\text{K}_x\text{Fe}_2\text{As}_2$ family, some understanding of the limits to the C_4 region need to be established. Similar high-resolution x-ray and high-intensity neutron diffraction experiments on a $x = 0.225(10)$ sample, with a temperature spacing of 2 K, show no evidence of a low-T tetragonal phase nor of any spin reorientation (Figure 6a

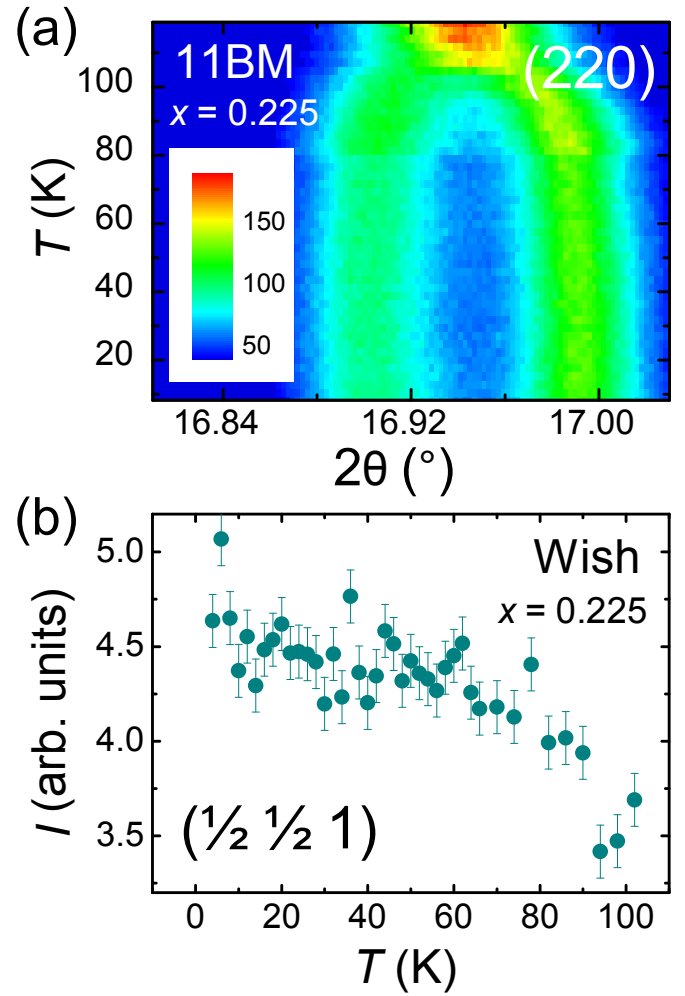


FIG. 6. Powder diffraction data from $\text{Ba}_{0.775}\text{K}_{0.225}\text{Fe}_2\text{As}_2$. (a) X-ray (11BM) diffractogram of the (220) reflection. (b) Integrated intensity across the $(\frac{1}{2} \frac{1}{2} 1)$ reflection from the neutron (Wish) diffraction data.

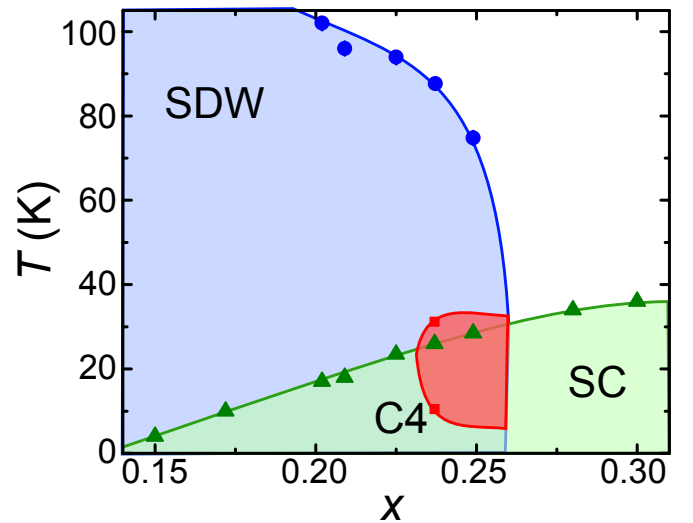


FIG. 7. Phase diagram of $\text{Ba}_{1-x}\text{K}_x\text{Fe}_2\text{As}_2$ revised from Ref. 11 to include the new diffraction data from this study.

and b, respectively), which sets a lower limit. While our previous report of high-resolution neutron diffraction¹¹ provides insufficient data to rule out the possibility that a small tetragonal phase appears below 40 K at $x = 0.25$, recent uniaxial dilatometry measurements provide evidence of a return to tetragonal symmetry in a narrow temperature range all the way up to the edge of the magnetic dome (in compositional space)¹⁵. While the application of stress may change the properties enough to shift phase boundary lines (for example, see Hassinger *et al.*¹⁶), this is consistent with our results, so the phase diagram of $\text{Ba}_{1-x}\text{K}_x\text{Fe}_2\text{As}_2$ is drawn to be consistent with this scenario in Figure 7. The complete suppression of the C_4 phase below T_c , shown in the inset to Fig. 5b, is consistent with our earlier observation that it competes more strongly with superconductivity than the C_2 phase.⁴

IV. CONCLUSION

The combined neutron and x-ray powder diffraction on $\text{Ba}_{0.76}\text{K}_{0.24}\text{Fe}_2\text{As}_2$ shows evidence of a second, minority phase below 30 K. The structural and magnetic features of the secondary phase indicate that it is the same as the previously reported tetragonal magnetic phase in $\text{Ba}_{1-x}\text{Na}_x\text{Fe}_2\text{As}_2$,⁴ but with a reduced stability range, possibly due to the larger cation size. This provides evidence that the C_4 phase is a universal feature of the hole-doped 122 family of iron-based superconductors. The resulting phase diagram is similar to the one recently re-

ported by Böhmer *et al.*¹⁵, although they claim that the tetragonal phase fraction is 100%. The fact that we observe it as a minority phase suggests that the stability of the C_4 phase is extremely sensitive to subtle changes in sample composition and measurement conditions. We have proposed that the C_4 phase is evidence for itinerant spin-nematic theory, in which the coupled magnetic and structural transitions are due to magnetic fluctuations caused by Fermi surface nesting. This theory predicts that the C_2 and C_4 phases have very similar free energies close to the suppression of C_2 order,⁴ which is consistent with the delicate stability of the C_4 phase. In this model, the C_4 SDW results from a simultaneous coupling between Fermi surfaces along two in-plane directions, rather than just one in the C_2 phase, providing a natural explanation for the stronger phase competition with superconductivity evident in the phase diagram.

ACKNOWLEDGMENTS

This work was supported by the U.S. Department of Energy, Office of Science, Materials Sciences and Engineering. This research used resources of the Advanced Photon Source, a U.S. Department of Energy (DOE) Office of Science User Facility operated for the DOE Office of Science by Argonne National Laboratory under Contract No. DE-AC02-06CH11357, and was aided by the 11-BM beam scientist M. Suchomel. Experiments at the ISIS Pulsed Neutron and Muon Source were supported by a beam time allocation from the Science and Technology Facilities Council.

* jallred@anl.gov

¹ H. Kontani, Y. Inoue, T. Saito, Y. Yamakawa, and S. Onari, Solid State Communications Special Issue on Iron-based Superconductors, **152**, 718 (2012).

² R. M. Fernandes, A. V. Chubukov, and J. Schmalian, Nature Physics **10**, 97 (2014).

³ P. Dai, J. Hu, and E. Dagotto, Nature Physics **8**, 709 (2012).

⁴ S. Avci, O. Chmaissem, J. M. Allred, S. Rosenkranz, I. Eremin, A. V. Chubukov, D. E. Bugaris, D. Y. Chung, M. G. Kanatzidis, J.-P. Castellán, J. A. Schlueter, H. Claus, D. D. Khalyavin, P. Manuel, A. Daoud-Aladine, and R. Osborn, Nature Communications **5**, 3845 (2014).

⁵ S. Avci, J. M. Allred, O. Chmaissem, D. Y. Chung, S. Rosenkranz, J. A. Schlueter, H. Claus, A. Daoud-Aladine, D. D. Khalyavin, P. Manuel, A. Llobet, M. R. Suchomel, M. G. Kanatzidis, and R. Osborn, Physical Review B (Condensed Matter and Materials Physics) **88**, 094510 (2013).

⁶ S. Avci, O. Chmaissem, E. A. Goremychkin, S. Rosenkranz, J.-P. Castellán, D. Y. Chung, I. S. Todorov, J. A. Schlueter, H. Claus, M. G. Kanatzidis, A. Daoud-Aladine, D. D. Khalyavin, and R. Osborn, Physical Review B (Condensed Matter and Materials

Physics) **83**, 172503 (2011).

⁷ F. Wasser, A. Schneidewind, Y. Sidis, S. Wurmehl, S. Aswartham, B. Buchner, and M. Braden, Physical Review B **91**, 060505 (2015).

⁸ D. D. Khalyavin, S. W. Lovesey, P. Manuel, F. Krüger, S. Rosenkranz, J. M. Allred, O. Chmaissem, and R. Osborn, Physical Review B **90**, 174511 (2014).

⁹ S. Nandi, M. G. Kim, A. Kreyssig, R. M. Fernandes, D. K. Pratt, A. Thaler, N. Ni, S. L. Bud'ko, P. C. Canfield, J. Schmalian, R. J. McQueeney, and A. I. Goldman, Physical Review Letters **104**, 057006 (2010).

¹⁰ M. Rotter, M. Pangerl, M. Tegel, and D. Johrendt, Angewandte Chemie International Edition **47**, 7949 (2008).

¹¹ S. Avci, O. Chmaissem, D. Y. Chung, S. Rosenkranz, E. A. Goremychkin, J.-P. Castellán, I. S. Todorov, J. A. Schlueter, H. Claus, A. Daoud-Aladine, D. D. Khalyavin, M. G. Kanatzidis, and R. Osborn, Physical Review B (Condensed Matter and Materials Physics) **85**, 184507 (2012).

¹² A. C. Larson and R. B. Von Dreele, Los Alamos National Laboratory Report **86-748** (2000).

¹³ B. H. Toby, J. Appl. Cryst. **34**, 210 (2001).

¹⁴ J. M. Allred, K. M. Taddei, D. E. Bugaris, S. Avci, D. Y. Chung, H. Claus, C. dela Cruz, M. G. Kanatzidis,

- S. Rosenkranz, R. Osborn, and O. Chmaissem, *Phys. Rev. B* **90**, 104513 (2014).
- ¹⁵ A. E. Böhrer, F. Hardy, L. Wang, T. Wolf, P. Schweiss, and C. Meingast, *ArXiv e-prints* (2014), arXiv:1412.7038 [cond-mat.supr-con].
- ¹⁶ E. Hassinger, G. Gredat, F. Valade, S. R. de Cotret, A. Juneau-Fecteau, J.-P. Reid, H. Kim, M. A. Tanatar, R. Prozorov, B. Shen, H. H. Wen, N. Doiron-Leyraud, and L. Taillefer, *Physical Review B (Condensed Matter and Materials Physics)* **86**, 140502 (2012).